



OPEN

# High-mobility ambipolar ZnO-graphene hybrid thin film transistors

SUBJECT AREAS:  
ELECTRONIC PROPERTIES  
AND DEVICES  
ELECTRONIC DEVICES

Wooseok Song, Soon Yeol Kwon, Sung Myung, Min Wook Jung, Seong Jun Kim, Bok Ki Min, Min-A Kang, Sung Ho Kim, Jongsun Lim & Ki-Seok An

Thin Film Materials Research Group, Korea Research Institute of Chemical Technology (KRICT), Yuseong P. O. Box 107, Daejeon 305-600, Republic of Korea.

Received  
19 November 2013

Accepted  
24 January 2014

Published  
11 February 2014

Correspondence and  
requests for materials  
should be addressed to  
K.-S.A. (ksan@kRICT.re.kr)

In order to combine advantages of ZnO thin film transistors (TFTs) with a high on-off ratio and graphene TFTs with extremely high carrier mobility, we present a facile methodology for fabricating ZnO thin film/graphene hybrid two-dimensional TFTs. Hybrid TFTs exhibited ambipolar behavior, an outstanding electron mobility of  $329.7 \pm 16.9 \text{ cm}^2/\text{V}\cdot\text{s}$ , and a high on-off ratio of  $10^5$ . The ambipolar behavior of the ZnO/graphene hybrid TFT with high electron mobility could be due to the superimposed density of states involving the donor states in the bandgap of ZnO thin films and the linear dispersion of monolayer graphene. We further established an applicable circuit model for understanding the improvement in carrier mobility of ZnO/graphene hybrid TFTs.

Together with the use of plastic substrates, solution processing for ZnO thin film transistors (TFTs) for flexible electronics has recently attracted attention owing to their light weight, low cost, transparency, and flexibility<sup>1</sup>. Unfortunately, it is widely recognized that the bottleneck of solution processed ZnO TFTs is the low carrier mobility. To overcome this problem, enormous efforts related to doping metal oxides with various metals have been undertaken<sup>2-4</sup>. Meanwhile, graphene, a two-dimensional  $sp^2$  bonded honeycomb lattice of carbon atoms, has emerged as a fascinating material for applications in next-generation nanoelectronics due to its high optical transmittance<sup>5</sup>, flexibility<sup>6</sup>, and extraordinary electronic properties, such as ambipolar conductance, ballistic transport over  $\sim 0.4 \mu\text{m}$  in length, half-integer quantum Hall effect, and extremely high carrier mobility at room temperature<sup>7-9</sup>. However, a limitation of graphene-based flexible TFTs is their semimetallic nature, specifically the gapless linear dispersion relation.

In this study, we combined the advantages of ZnO TFTs with a high on-off ratio and graphene TFTs with extremely high carrier mobility for the realization of high-performance TFTs. Thus far, several approaches for the formation of semiconductor-graphene hybrid nanostructures have focused on applications in optoelectronics and photocatalysts<sup>10-18</sup>. We established a facile methodology for fabricating high-performance ZnO/graphene hybrid TFTs and explored the origin of the improvement in carrier mobility of hybrid TFTs.

## Results

**Formation of ZnO/graphene hybrid nanostructure.** The thickness of a ZnO film formed by 20 coating cycles is estimated to be  $\sim 72 \text{ nm}$  (Fig. 1a). The ZnO thin film possesses a flat surface and uniform thickness. In addition, the thickness and the surface morphology of the ZnO film and the ZnO/graphene hybrid film are almost similar (Supplementary Fig. S1). The thickness of the ZnO film can be controlled by adjusting the number of coating cycles. Based on SEM observations, the ZnO film thicknesses were 22, 47 and 72 nm, corresponding to coating cycles of 5, 10, and 20, respectively (Supplementary Fig. S2). The formation of a ZnO/graphene hybrid film was implemented as follows. First, graphene was synthesized on Cu using a conventional TCVD system. The graphene film was transferred onto a  $\text{SiO}_2$  (300 nm)/Si(001) substrate by a poly(methyl methacrylate) (PMMA)-assisted wet-transfer method. Solution-processed ZnO thin films with controlled thickness were spin-coated onto the graphene/ $\text{SiO}_2$ /Si substrates. A schematic diagram of the ZnO/graphene hybrid film is shown (Fig. 1b). The optical transmittances at 550 nm of graphene, ZnO (20 cycles), and ZnO (20 cycles)/graphene are 97.1, 95.0, and 93.6%, respectively. Considering the opacities of monolayer graphene ( $2.3 \pm 0.1\%$ ) and ZnO thin film<sup>5,19</sup>, the synthesis of monolayer graphene and the formation of highly transparent ZnO/graphene hybrid films were manifested (Fig. 1c). Hybrid materials are required for TFTs in transparent and flexible electronic applications. The Raman spectra of graphene and ZnO/graphene, exhibiting that the graphene fingerprints: the D-, G-, and 2D-bands were clearly observed (Fig. 1d,e). The G-band is associated

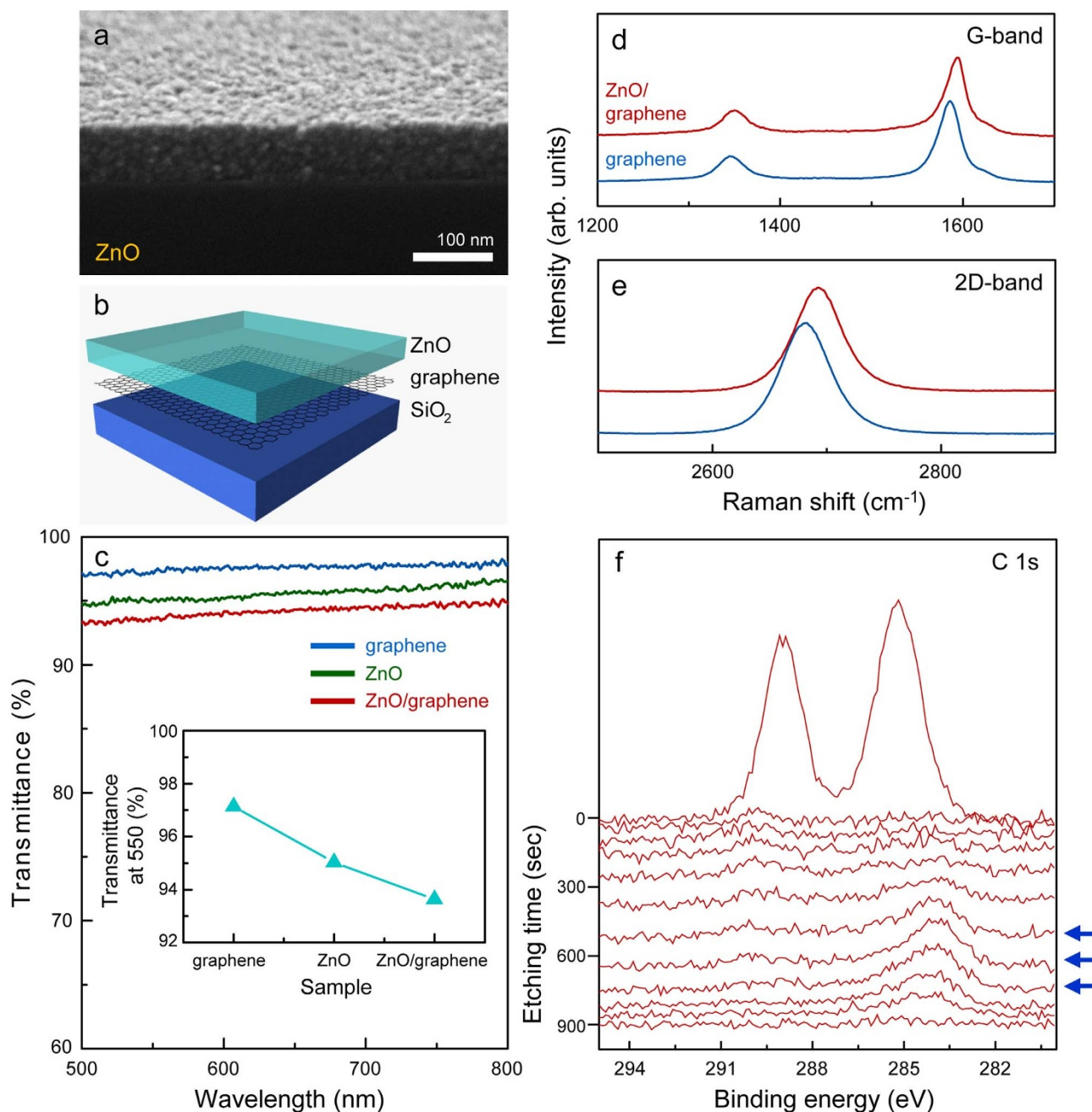


**Figure 1** | (a) SEM image for solution-processed ZnO thin film on SiO<sub>2</sub> (300 nm)/Si(001) substrate. (b) A schematic diagram of ZnO/graphene hybrid film. (c) Optical transmittance of graphene, ZnO, and ZnO/graphene. The inset compares the transmittance at 550 nm for different samples. (d) G-band and (e) 2D-band spectra with an excitation wavelength of 514 nm for graphene and ZnO/graphene hybrid film. (f) Evolution of the C 1s core level spectra of ZnO/graphene hybrid film as a function of etching time.

with a normal first order Raman scattering involving an electron and the doubly degenerated phonons (*i*TO and *i*LO) at the Brillouin zone center<sup>20</sup>. Furthermore, the 2D-band originated from an intervalley double resonance Raman process involving an electron and two *i*TO phonons at the K point<sup>20</sup>. The G- and 2D-bands experience a significant blueshift after the formation of the ZnO/graphene hybrid film. Together, the intensity ratio of the 2D- to G-band ( $I_{2D}/I_G$ ) significantly decreased from  $2.72 \pm 0.13$  to  $2.46 \pm 0.08$ . The position of the G- and 2D-bands and the  $I_{2D}/I_G$  are summarized (Supplementary Fig. S3). These results can be adequately explained by a work function difference between the ZnO thin film (5.1–5.3 eV) and graphene (4.5–4.8 eV)<sup>21,22</sup>, which allowed electron charge transfer from graphene to ZnO. Moreover,

the intensity ratio of the D- to G-band increased after the formation of the ZnO/graphene hybrid film, which is attributed to structural deformation of the sp<sup>2</sup> carbon network induced by ZnO/graphene hybridization (Supplementary Fig. S4). An evolution of the XPS C 1s core level spectra of the ZnO/graphene hybrid film as a function of Ar<sup>+</sup> etching for depth profiling. The carbon contamination is observed only at the outermost surface. The sp<sup>2</sup> C-C bond and a small amount of C-O and C=O bonds for graphene were observed at etching time for 500 sec (denoted by blue arrows)<sup>23</sup>. Notably, an atomically abrupt interface between the ZnO thin film and graphene without the PMMA residue is found (Fig. 1f). Additionally, the Zn 2p, Si 2p, and O 1s core level spectra of the ZnO/graphene hybrid film were obtained (Supplementary Fig. S4). The shifts of the binding

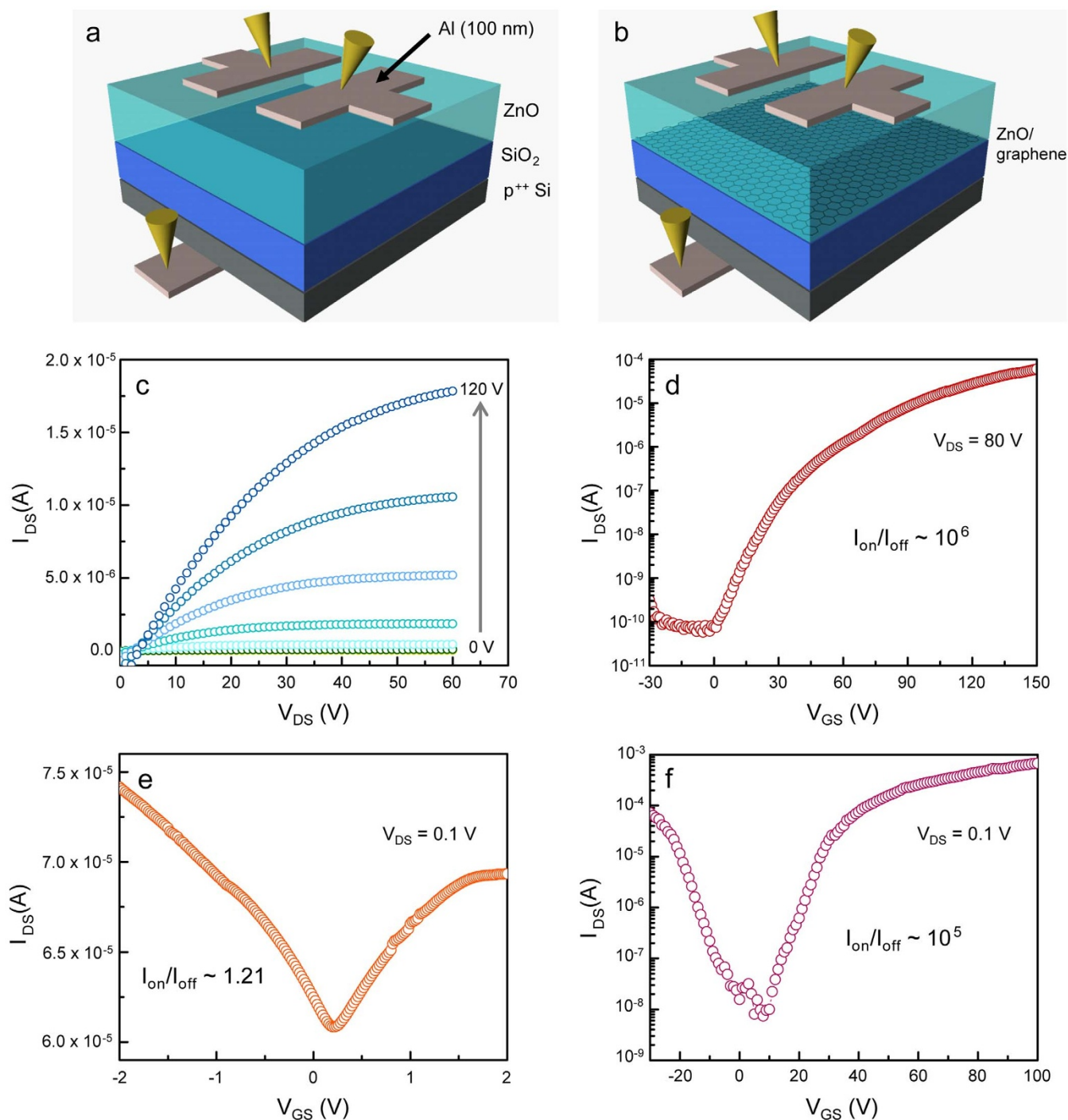


**Figure 2** | Schematic illustration of the device structure, including the bottom-gate configuration, 300 nm-thick SiO<sub>2</sub> gate dielectric, and 100 nm-thick Al source/drain contacts for (a) ZnO TFTs and (b) ZnO/graphene hybrid TFTs. (c) Output characteristic of ZnO TFTs at room temperature. Transfer characteristics of (d) ZnO TFTs, (e) electrochemically gate tuned graphene TFTs, and (f) ZnO/graphene TFTs.

energy were observed in the core level spectra of Si 2p and O 1s (Si-O bonding). This can be explained by band bending effects induced by the formation of ZnO/graphene. In contrast, there are no noticeable changes in a Zn-O bonding component in the core level spectra of O 1s.

**Electrical transport properties of ZnO and ZnO/graphene TFTs.** Schematics of the ZnO and ZnO/graphene hybrid TFTs are depicted (Fig. 2a,b). The ZnO thin film and ZnO/graphene hybrid film were both used as the channel and heavily p-doped silicon wafers were employed as the gate electrode. The gate dielectric layer is

300-nm-thick SiO<sub>2</sub>. Aluminum (100 nm-thick) source and drain electrodes were deposited by thermal evaporation through a shadow mask. The channel length and width are 200 and 1735 μm, respectively. All transistors were measured in the dark under ambient conditions. Drain current ( $I_{DS}$ )-drain voltage ( $V_{DS}$ ) relations at various gate voltages ( $V_{GS}$ ), revealing that a typical accumulation mode n-channel transistor behavior can be seen: a linear regime and a saturation regime are both observed (Fig. 2c). A representative transfer characteristic ( $I_{DS}$ - $V_{GS}$ ) at  $V_{DS} = 80$  V of the ZnO TFTs is shown (Fig. 2d), exhibiting unipolar n-channel transistor behavior with an on-off ratio of  $10^6$ . For comparison, we

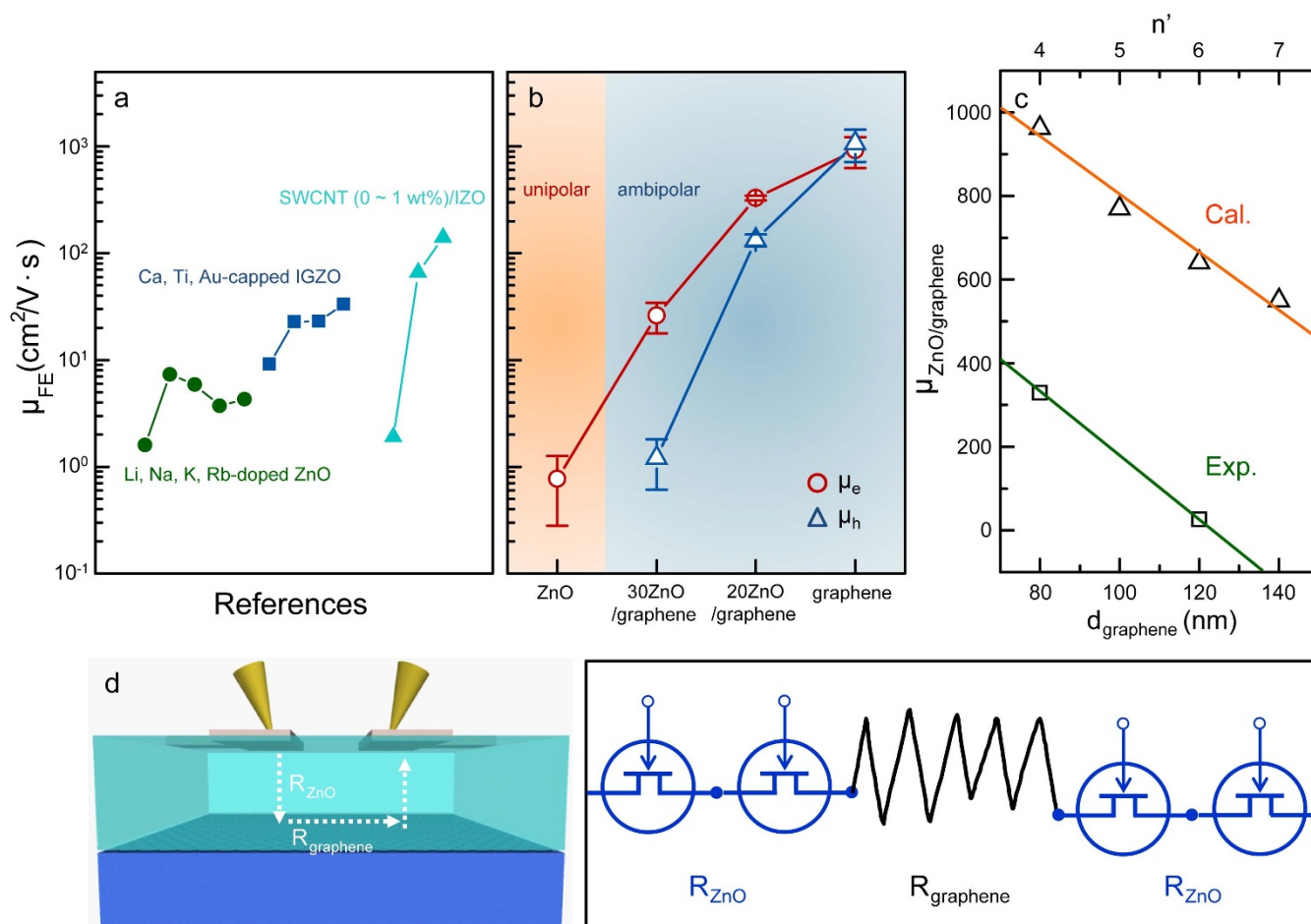


**Figure 3** | Plot of the  $\mu_{FE}$  vs. ZnO thin film doped with various materials: (a) previously reported materials and (b) the  $\mu_e$  and  $\mu_h$  for the ZnO thin film, thickness-controlled ZnO/graphene, and graphene (this work). (c) Relationship between  $\mu_{ZnO/graphene}$  and graphene depth in the ZnO/graphene hybrid film. (d) Schematic diagrams of the conducting path of charged particles in ZnO/graphene hybrid TFTs and the simplified circuit diagrams of the nanostructured ZnO/graphene hybrid TFTs.

also fabricated electrochemically-gated graphene TFTs<sup>24</sup> because it is difficult to observe the charge-neutral Dirac point (CNBP) in the transfer curve for graphene-based TFTs with a bottom gate configuration (Supplementary Fig. S5)<sup>25</sup>. The transfer curve of the electrochemically-gated graphene TFTs at  $V_{DS} = 0.1$  V exhibits ambipolar behavior with an on-off ratio of 1.21 and a CNBP at 0.2 V due to the unintentional p-type doping of graphene from water molecules (Fig. 2e)<sup>26</sup>. This unintentional doping also caused an asymmetric maximum  $I_{DS}$  of electrons and holes in the ON state. Interestingly, the ZnO/graphene hybrid TFT shows clear ambipolar behavior with an on-off ratio of 10<sup>5</sup>, as shown (Fig. 2f). The off current state of the ZnO/graphene hybrid TFT decreases significantly compared with that of the graphene TFT. This transistor behavior can be observed at  $V_{DS} = 0.1$  V, whereas the ZnO TFT did not exhibit switching behavior at  $V_{DS} = 0.1$  V (not shown here).

## Discussion

In general, an ambipolar device is hole conducting (p channel) when a negative  $V_{GS}$  is applied and is electron conducting (n channel) when a positive  $V_{GS}$  is applied. The transfer characteristics reflect the density of states (DOS) near the Fermi level of channel materials. We believe that the ambipolar behavior of the ZnO/graphene hybrid TFT can be adequately explained by the superimposed DOS involving the donor states in the bandgap of the ZnO thin film and the linear dispersion of monolayer graphene with an electron energy  $E(k) = \hbar v_F k$ , where  $v_F$  is the Fermi velocity and  $k$  is the electron wave vector. Along these lines, the conduction of electrons in the ZnO/

graphene hybrid TFT is greater than that of the holes, unlike unintentionally p-type doped graphene-based TFTs. It is notable that previous studies on the transfer characteristics of carbon nanotube p-n junction diodes<sup>27</sup> and p-n junctions in liquid-gated ambipolar MoS<sub>2</sub> transistors<sup>28</sup> also revealed a combined feature of the donor states in the bandgap of n-type semiconductors and the acceptor states in the bandgap of p-type semiconductors, namely, ambipolar behavior.

Based on the transfer curves, the field effect mobilities ( $\mu_{FE}$ ) were calculated by the relationship<sup>29</sup>:

$$\mu_{FE} = \frac{Lg_m}{V_{DS}C_iW}$$

where  $C_i$  (11.6 nF/cm<sup>2</sup>)<sup>30</sup> and  $g_m$  are the gate capacitance per unit area and the transconductance, respectively. Surprisingly, the electron and hole mobilities ( $\mu_e$  and  $\mu_h$ ) of ambipolar ZnO film/graphene hybrid TFTs formed after 20 coating cycles (20ZnO/graphene) are dramatically improved to  $329.7 \pm 16.9$  cm<sup>2</sup>/V·s and  $133 \pm 17$  cm<sup>2</sup>/V·s, respectively, compared to those ( $\mu_e = 0.77 \pm 0.49$  cm<sup>2</sup>/V·s) for the TFTs with a unipolar ZnO channel, which is significantly larger than those of Li, Na, K, Rb-doped ZnO ( $1.6 \sim 7.3$  cm<sup>2</sup>/V·s)<sup>31</sup>, Ca, Ti, Au-capped IGZO ( $9.2 \sim 33.2$  cm<sup>2</sup>/V·s)<sup>32</sup>, and carbon nanotube incorporated IZO ( $1.9 \sim 140$  cm<sup>2</sup>/V·s) (Fig. 3a,b)<sup>33</sup>. This is mainly due to the superimposed DOS reflecting both the n-type behavior of the ZnO thin film and the unusual electronic structure of graphene. In particular, the Fermi velocity  $v_F$  is  $1.05 \times 10^6$  m/s<sup>34</sup>, as extracted



from the slope of the linear dispersion of graphene; this affects the carrier mobility in the hybrid TFTs. Additionally, the  $\mu_e$  and  $\mu_h$  of the ZnO film formed by 30 cycles of coating/graphene hybrid TFTs (30ZnO/graphene) are  $26.06 \pm 8.26 \text{ cm}^2/\text{V}\cdot\text{s}$  and  $1.21 \pm 0.6 \text{ cm}^2/\text{V}\cdot\text{s}$ , respectively. For the graphene TFTs, the mobility becomes larger for holes ( $1076 \pm 359 \text{ cm}^2/\text{V}\cdot\text{s}$ ) than electrons ( $926 \pm 296 \text{ cm}^2/\text{V}\cdot\text{s}$ ). From an electronic circuit standpoint, we established an applicable model. Firstly, the conducting path of the charged particles in the ZnO/graphene hybrid TFTs seems to be  $\text{ZnO} \rightarrow \text{graphene} \rightarrow \text{ZnO}$ , because the graphene has a low resistance (Fig. 3d). Secondly, we considered the simplified circuit model that the ZnO thin film TFT consists of  $n$  parts of an individual ZnO TFT, and the ZnO thin film/graphene hybrid TFT consists of  $n'$  parts of an individual ZnO TFT since the resistance of graphene here can be ignored compared with that of the ZnO thin films. Namely, the field effect mobility of the ZnO thin film/graphene hybrid TFTs ( $\mu_{\text{ZnO/graphene}}$ ) is limited only by the in-grain and grain boundary scatterings on the ZnO thin films. Thus, the  $\mu_{\text{ZnO/graphene}}$  is described by the relationship<sup>33</sup>:

$$\frac{\mu_{\text{ZnO/graphene}}}{\mu_{\text{ZnO}}} = \frac{g_{\text{mZnO/graphene}}}{g_{\text{mZnO}}} = \frac{n'}{n}$$

In our system, the grain sizes of ZnO thin films are approximately 40 nm (Supplementary Fig. S6). Thus, the channel of ZnO thin film TFT contains 5000 individual ZnO TFTs, whereas the channel of ZnO thin film/graphene hybrid TFTs contains 4 individual ZnO TFTs (the conducting path of electrons being:  $2 \text{ ZnO} \rightarrow \text{graphene} \rightarrow 2 \text{ ZnO}$ ) due to the ZnO thin film thickness (80 nm), in which the mobility enhancement factor ( $n'/n$ ) is 1250. The experimental and calculated values for  $\mu_{\text{ZnO/graphene}}$  as a function of the graphene depth ( $d_{\text{graphene}}$ ; ZnO thin film thickness) in the ZnO/graphene hybrid film, which is associated with the  $n'$  parts of individual ZnO TFTs, were plotted (Fig. 3c). This result suggests that the two lines have a similar trend, indicating that our suggestion is reasonable. We anticipate that this discrepancy between the experimental and calculated values can be understood by the fact that the resistance of graphene is mainly due to carrier scattering at graphene grain boundaries and the fact that the contact resistance between the ZnO thin film and graphene were ignored. Additionally, assuming linear dependence between the experimental values for  $\mu_{\text{ZnO/graphene}}$  and  $d_{\text{graphene}}$ , the extrapolated mobility at  $d_{\text{graphene}} = 0$  is  $934.8 \text{ cm}^2/\text{V}\cdot\text{s}$  which is similar to the mobility extracted from the graphene TFT ( $926 \text{ cm}^2/\text{V}\cdot\text{s}$ ) (Fig. 2e), indicating that our suggested model is reasonable.

In conclusion, we established a facile methodology for fabricating ZnO thin film/graphene hybrid two-dimensional TFTs. The ambipolar ZnO/graphene hybrid TFTs show outstanding carrier mobility ( $329.7 \pm 16.9 \text{ cm}^2/\text{V}\cdot\text{s}$ ), a high on-off ratio ( $10^5$ ), and facile processability, including solution processing and easy wet transfer. We further studied the origin of the ambipolar behavior of ZnO/graphene hybrid TFT with high electron mobility using the superimposed DOS concept and an applicable circuit model. Notably, these results open new opportunities not possible with ZnO-based TFTs in terms of their carrier mobility. In addition, the ZnO/graphene hybrid TFTs may be suitable for multifaceted applications that require low cost, a large area, transparency, and mechanical flexibility.

## Methods

**CVD growth of graphene.** Graphene was synthesized using conventional thermal chemical vapor deposition (TCVD). A 25- $\mu\text{m}$ -thick Cu foil (Alfa Aesar, 99.8% purity) was used as a catalytic substrate for graphene growth. The Cu foil was heated to  $1050^\circ\text{C}$  inside the TCVD reactor under 100 sccm flow of  $\text{H}_2$  gas at a pressure of  $\sim 5$  Torr for 60 min. After this pre-annealing process, which was crucial for enlarging the Cu grains and establishing a smooth surface,  $\text{CH}_4$  (2 sccm) was introduced as a carbon feedstock with  $\text{H}_2$  gas for 25 min to obtain graphene. The  $\text{CH}_4$  gas was then turned off, and the TCVD reactor was cooled to room temperature under a flow of  $\text{H}_2$  gas. The synthesized graphene films were transferred onto  $\text{SiO}_2$  (300 nm)/ $\text{Si}(001)$  substrates by a poly(methyl methacrylate)(PMMA)-assisted wet-transfer method<sup>35</sup>.

**Fabrication of the ZnO/graphene hybrid films.** A single coating cycle for the formation of ZnO thin film/graphene consists of the following steps: the 0.05 M zinc acetate dehydrate ( $\text{Zn}(\text{O}_2\text{CCH}_3)_2 \cdot 2\text{H}_2\text{O}$ ) was stirred in 2-methoxyethanol at  $70^\circ\text{C}$  for 5 min. A dilute ZnO solution was spin-coated onto the graphene/ $\text{SiO}_2/\text{Si}$  substrates, in which the substrate rotation speed and time were 2000 rpm and 30 seconds, respectively. Then, the substrate was immediately cured at  $150^\circ\text{C}$  for 1 min. The number of repeated coating cycles, consisting of spin-coating and curing processes, was adjusted in the range of 10 to 30, which is critical for controlling the thickness of ZnO thin films. The resulting films were post-annealed at  $300^\circ\text{C}$  for 1 h under ambient conditions.

- Song, K. *et al.* Fully Flexible solution-deposited ZnO thin-film transistors. *Adv. Mater.* **22**, 4308–4312 (2010).
- Adamopoulos, G. *et al.* Spray-deposited Li-doped ZnO transistors with electron mobility exceeding  $50 \text{ cm}^2/\text{Vs}$ . *Adv. Mater.* **22**, 4764–4769 (2010).
- Adamopoulos, G. *et al.* High-mobility low-voltage ZnO and Li-doped ZnO transistors based on  $\text{ZrO}_2$  high-k dielectric grown by spray pyrolysis in ambient air. *Adv. Mater.* **23**, 1894–1898 (2011).
- Park, S. Y. *et al.* The structural, optical, and electrical characterization of high-performance, low-temperature and solution-processed alkali metal-doped ZnO TFTs. *J. Mater. Chem. C* **1**, 1383–1391 (2013).
- Nair, R. R. *et al.* Fine structure constant defines visual transparency of graphene. *Science* **320**, 1308 (2008).
- Kim, K. S. *et al.* Large-scale pattern growth of graphene films for stretchable transparent electrodes. *Nature* **457**, 706–710 (2009).
- Novoselov, K. S. *et al.* Electric field effect in atomically thin carbon films. *Science* **306**, 666–669 (2004).
- Zhang, Y., Tan, Y.-W., Stormer, H. L. & Kim, P. Experimental observation of the quantum Hall effect and Berry's phase in graphene. *Nature* **438**, 201–204 (2005).
- Novoselov, K. S. *et al.* Room-temperature quantum Hall effect in graphene. *Science* **315**, 1379 (2007).
- Son, D. I. *et al.* Emissive ZnO-graphene quantum dots for white-light-emitting diodes. *Nat. Nanotechnol.* **7**, 465–471 (2012).
- Fu, X.-W. *et al.* Graphene/ZnO nanowire/graphene vertical structure based fast-response ultraviolet photodetector. *Appl. Phys. Lett.* **100**, 223114 (2012).
- Zhang, N., Zhang, Y. & Xu, Y.-J. Recent progress on graphene-based photocatalysts: current status and future perspectives. *Nanoscale* **4**, 5792–5813 (2012).
- Yang, M.-Q. & Xu, Y.-J. Selective photoredox using graphene-based composite photocatalysts. *Phys. Chem. Chem. Phys.* **15**, 19102–19118 (2013).
- Zhang, Y., Tang, Z.-R., Fu, X. & Xu, Y.-J.  $\text{TiO}_2$ -graphene nanocomposites for gas-phase photocatalytic degradation of volatile aromatic pollutant: is  $\text{TiO}_2$ -graphene truly different from other  $\text{TiO}_2$ -carbon composite materials? *ACS Nano* **4**, 7303–7314 (2010).
- Zhang, Y., Tang, Z.-R., Fu, X. & Xu, Y.-J. Engineering the unique 2D mat of graphene to achieve graphene- $\text{TiO}_2$  nanocomposite for photocatalytic selective transformation: what advantage does graphene have over its forebear carbon nanotube? *ACS Nano* **5**, 7426–7435 (2011).
- Zhang, Y., Zhang, N., Tang, Z.-R. & Xu, Y.-J. Graphene transforms wide band gap ZnS to a visible light photocatalyst. The new role of graphene as a macromolecular photosensitizer. *ACS Nano* **6**, 9777–9789 (2012).
- Kim, Y.-J. *et al.* Hydrothermally grown ZnO nanostructures on few-layer graphene sheets. *Nanotechnology* **22**, 245603 (2011).
- Lin, J. *et al.* Heterogeneous graphene nanostructures: ZnO nanostructures grown on large-area graphene layers. *Small* **6**, 2448 (2010).
- Fortunato, E. M. C. *et al.* Fully transparent ZnO thin-film transistor produced at room temperature. *Adv. Mater.* **17**, 590–594 (2005).
- Malard, L. M., Pimenta, M. A., Dresselhaus, G. & Dresselhaus, M. S. Raman spectroscopy in graphene. *Phys. Rep.* **473**, 51–87 (2009).
- You, J. B. *et al.* Enhancement of field emission of the ZnO film by the reduced work function and the increased conductivity via hydrogen plasma treatment. *Appl. Phys. Lett.* **94**, 262105 (2009).
- Yu, Y.-J. *et al.* Tuning the graphene work function by electric field effect. *Nano Lett.* **9**, 3430–3434 (2009).
- Luo, Z. *et al.* Modulating the electronic structures of graphene by controllable hydrogenation. *Appl. Phys. Lett.* **97**, 233111 (2010).
- Song, W. *et al.* Site-specific growth of width-tailored graphene nanoribbons on insulating substrates. *J. Phys. Chem. C* **116**, 20023–20029 (2012).
- Song, W. *et al.* Homogeneous and stable p-type doping of graphene by MeV electron beam-stimulated hybridization with ZnO thin films. *Appl. Phys. Lett.* **102**, 053103 (2013).
- Ryu, S. *et al.* Atmospheric oxygen binding and hole doping in deformed graphene on a  $\text{SiO}_2$  substrate. *Nano Lett.* **10**, 4944–4951 (2010).
- Lee, J. U., Gipp, P. P. & Heller, C. M. Carbon nanotube p-n junction diodes. *Appl. Phys. Lett.* **85**, 145–147 (2004).
- Zhang, Y. J., Ye, J. T., Yomogida, Y., Takenobu, T. & Iwasa, Y. Formation of a stable p-n junction in a liquid-gated  $\text{MoS}_2$  ambipolar transistor. *Nano Lett.* **13**, 3023–3028 (2013).
- Ortel, M., Pittner, S. & Wagner, V. Stability and spacial trap state distribution of solution processed ZnO-thin film transistors. *J. Appl. Phys.* **113**, 154502 (2013).



30. Farmer, D. B., Lin, Y.-M. & Avouris, P. Graphene field-effect transistors with self-aligned gates. *Appl. Phys. Lett.* **97**, 013103 (2010).
31. Park, S. Y. *et al.* Low-temperature, solution-processed and alkali metal doped ZnO for high-performance thin-film transistors. *Adv. Mater.* **24**, 834–838 (2012).
32. Zan, H.-W. *et al.* Dual gate indium-gallium-zinc-oxide thin film transistor with an unisolated floating metal gate for threshold voltage modulation and mobility enhancement. *Appl. Phys. Lett.* **98**, 153506 (2011).
33. Liu, X. *et al.* Rational design of amorphous indium zinc oxide/carbon nanotubes hybrid film for unique performance transistors. *Nano Lett.* **12**, 3596–3601 (2012).
34. Elias, D. C. *et al.* Dirac cones reshaped by interaction effects in suspended graphene. *Nat. Phys.* **7**, 701–704 (2011).
35. Li, X. *et al.* Transfer of large-area graphene films for high-performance transparent conductive electrodes. *Nano Lett.* **9**, 4359–4363 (2009).

## Acknowledgments

This research was supported by the Converging Research Center Program through the Ministry of Science, ICT and Future Planning, Korea (2013K000162) and by a grant (2011-0031636) from the Center for Advanced Soft Electronics under the Global Frontier Research Program of the Ministry of Science, ICT and Future Planning, Korea.

## Author contributions

W.S. analyzed data and wrote the manuscript, S.Y.K., M.W.J., S.J.K., B.K.M., M.-A.K., S.H.K. performed the experiments, S.M, J.L., K.-S.A. proposed and supervised the research. All authors participated in discussions of the research.

## Additional information

**Supplementary information** accompanies this paper at <http://www.nature.com/scientificreports>

**Competing financial interests:** The authors declare no competing financial interests.

**How to cite this article:** Song, W. *et al.* High-mobility ambipolar ZnO-graphene hybrid thin film transistors. *Sci. Rep.* **4**, 4064; DOI:10.1038/srep04064 (2014).



This work is licensed under a Creative Commons Attribution-NonCommercial-ShareAlike 3.0 Unported license. To view a copy of this license, visit <http://creativecommons.org/licenses/by-nc-sa/3.0>